Supplementary Material for

Eco-Evolutionary Dynamics of a Population with Randomly Switching Carrying Capacity

Karl Wienand*, Erwin Frey*, and Mauro Mobilia†

In this Supplementary Material, we provide comments concerning the dichotomous noise, notes on the methodology and data avalability, the derivation of the probability densities of the piecewise-deterministic Markov process (PDMP), complementary results about the mean fixation times, as well as additional discussions about the PDMP approximation and the emergence of cooperation in the eco-evolutionary game, and additional technical details concerning the linear noise approximation to the population size's quasi-stationary distribution.

In what follows, unless stated otherwise, the notation is the same as in the main text and the equations and figures refer to those therein. (As in the main text, unless explicitly mentioned otherwise, below we tacitly assume $x_0 = 1/2$.)

1 Relationship between dichotomous Markov noise and other forms of environmental noise

It is worth outlining some of the similarities and differences between the dichotomous Markov Noise (DMN) and the Ornstein-Uhlenbeck process (OUP) that is also commonly used to model environmental noise, see *e.g.* [1]. Both are *colored noises* with exponential auto-correlation functions, see Sec. II in the main text and Refs. [2, 3]. However, while the Ornstein-Uhlenbeck Process is a Gaussian and unbounded process, the DMN is, in general, *neither*. In fact, the piecewise-deterministic Markov process (PDMP) [4]

$$\dot{N} = N\left(1 + q - \frac{N}{\mathcal{K}}\right) + \Delta\xi, \tag{S1}$$

with the DMN ξ, becomes a diffusive process with Gaussian white noise and diffusion constant $D = \Delta^2/\nu$ only in the limit of $\Delta \to \infty, \nu \to \infty$ and $0 < D < \infty$, see, *e.g.*, Refs. [2, 3, 5]. The PDMP that we consider in this work has the form:

$$\dot{N} = \mathcal{F}(N,\xi) = \begin{cases} \mathcal{F}_+(N) & \text{if } \xi = 1 \\ \mathcal{F}_-(N) & \text{if } \xi = -1 \end{cases} \quad \text{with} \quad \mathcal{F}_\pm(N) \equiv N\left[1 + q - \frac{N}{K_\pm}\right], \tag{S2}$$

which is identical to (S1) with $\Delta = (K_+ - K_-)/(2K_+K_-)$. Since $K_+ > K_- \gg 1$, the Gaussian white noise limit is unphysical, and the PDMP that we consider in this work is therefore *never diffusive*.

It is also worth noting that, being bounded, the DMN has the great advantage of guaranteeing that the fluctuating carrying capacity $K(t) = [(K_+ + K_-) + \xi(t)(K_+ - K_-)]/2$ remains always finite and positive, which would not be the case if $\xi(t)$ was given by an OUP. Furthermore, the DMN can be considered a discrete-step approximation [2, 3] of the OUP, but is more mathematically tractable and easier to simulate.

2 Notes on methodology & Data availability

Source code for all simulations, resulting data and the *Mathematica* notebook [6] used for calculations and figures are available electronically along as *figshare* resources [7].

2.1 Stochastic simulations

Using Gillespie's stochastic simulation algorithm (SSA) [8], we have simulated exactly the dynamics described by the master equation (5). To efficiently ensure that quasi-stationarity was reached [9], we have run individual-based simulations until fixation occurred in 99% of the realizations (for $\nu \gtrsim s$), or until time reaches $t = 10/\nu$ (when

*Arnold Sommerfeld Center for Theoretical Physics, Department of Physics, Ludwig-Maximilians-Universität München, Theresienstrasse 37, 80333 München, Germany. *Email: karl.wienand@physik.lmu.de, Frey@lmu.de*

† Department of Applied Mathematics, School of Mathematics, University of Leeds, Leeds LS2 9JT, U.K. *Email: M.Mobilia@leeds.ac.uk*

$\nu \ll s$). We have simulated ensembles of 10^4 realizations of the system, except to determine the various population size distributions (for which we used a larger sample of 10^5 realizations) and when using "high values" of s (i.e. for $s = \mathcal{O}(1)$ as in figure S2)(b,c). In this case, an even larger sample of 10^6 realizations was needed to accurately estimate the fixation probability of S.

2.2 Numerical limitations on effective parameter $q(b)$ approach

To obtain the parameter $q(b)$ used in the formula for ϕ_q, we first recorded the fixation probability from SSA results with constant $K = \mathcal{K}$, $b \in \{0.1k : k \in \mathbb{N}, k \leq 100\}$, and $s \in \{0.02, 0.05\}$ (10^6 runs each). For each combination of parameters, we computed $q(b)$ by matching the fixation probability $\phi|_{(1+q)\mathcal{K}}$ of the fitness-dependent Moran model, see equation (12) in Sec. III.B also given by eq. (S13) below, with the corresponding fixation probability obtained in the SSA result.

The values of $q(b)$ have then been used to compute ϕ_q according to equation (S11) for several values of ν, as shown in figure 3(b). Due to numerical instabilities in the evaluation of stationary distribution $p^*_{\nu,q}$ in Mathematica [6], numerical evaluations of ϕ_q occasionally "failed" or produced outliers. Data corresponding to these occasional issues were omitted (without statistical consequences) from our dataset. This has sometimes led to some gaps in the lines of the analytical predictions (see *e.g.* the green curve in figure 3 (b)). Furthermore, $q(b)$ has only been determined for a discrete set of b values, which limits the resolution in determining b_c and b^*. Specifically, since the spacing between the values used for b was 0.1, neither b^* nor b_c has been determined with an accuracy higher than 0.1. The combination of limited resolution and outliers causes the jaggedness observed in figure S7(a) for the graph of b^* obtained by looking for the maximum of equation (21).

2.3 Data availability: Mathematica notebook & Linear noise approximation figures 7 and 8

The direct numerical evaluation of equations (S39) and (S40), used to generate the figures 7 and 8, is commented in the accompanying Mathematica notebook [7].

3 Joint and marginal stationary PDFs of the auxiliary PDMP (9)

In the main text, we have frequently used of the marginal stationary probability density function (PDF) of the single-variate PDMP (9) that reads

$$p^*_{\nu,q}(N) = \frac{\mathcal{Z}_{\nu,q}}{N^2} \left[\frac{(N^*_+ - N)(N - N^*_-)}{N^2}\right]^{\frac{\nu}{1+q}-1}. \tag{S3}$$

When $b = q = 0$, we have $p^*_{\nu,0}(N) \equiv p^*_\nu(N) = \frac{\mathcal{Z}_\nu}{N^2} \left[\frac{(K_+ - N)(N - K_-)}{N^2}\right]^{\nu-1}$.

In this section, we outline the derivation of this PDF, as well as that of the joint stationary probability density $p^*_{\nu,q}(N, \xi)$ of N and ξ. For notational simplicity, in the remainder of this section, we write $p_{\nu,q} = p$ and $p^*_{\nu,q} = p^*$. It follows from the Chapman-Kolmogorov equation, that $p(N, \xi)$ obeys the master-like equation [2]

$$\partial_t p(N, \xi, t) = -\partial_N \left[\mathcal{F}(N, \xi) p(N, \xi, t)\right] - \nu \left[p(N, \xi, t) - p(N, -\xi, t)\right], \tag{S4}$$

which can conveniently be rewritten as $\partial_t p(N, \xi, t) = -\partial_N J(N, \xi, t)$ in terms of the probability current [11]

$$J(N, \xi, t) = \mathcal{F}(N, \xi) p(N, \xi, t) \quad + \quad \nu \int_{N^*_-}^{N} dN' \left[p(N', \xi, t) - p(N', -\xi, t)\right]. \tag{S5}$$

The first term on the right-hand-side (RHS) of (S5) accounts for the probability flowing outside $[N^*_-, N]$ (Liouvillian flow), whereas the second accounts for the random switching. At stationarity, $\lim_{t\to\infty} p(N, \xi, t) = p^*(N, \xi)$ and $\lim_{t\to\infty} J(N, \xi, t) = J^*(N, \xi)$, with $\partial_t p^*(N, \xi) = -\partial_N J^*(N, \xi) = 0$, which implies $\partial_N (J^*(N, \xi) + J^*(N, -\xi)) = 0$. With the (natural) zero-current boundary conditions at $N^*_\pm$ [2], i.e. $J^*(N, \xi) = 0$, we find a simple relationship between the PDFs in each of the environmental states:

$$p^*(N, \xi) = -\left(\frac{\mathcal{F}(N, -\xi)}{\mathcal{F}(N, \xi)}\right) p^*(N, -\xi). \tag{S6}$$

With this relation, $\partial_N J^*(N,-\xi)=0$ gives

$$0=\partial_N\left[\mathcal{F}(N,-\xi)p^*(N,-\xi)\right]+\nu\left[\frac{1}{\mathcal{F}(N,-\xi)}+\frac{1}{\mathcal{F}(N,\xi)}\right]\left(\mathcal{F}(N,-\xi)p^*(N,-\xi)\right).$$

Combined with equation (S6), this readily yields $p^*(N,\xi)\propto\pm\mathfrak{g}(N)/\mathcal{F}(N,\xi)$, where

$$\mathfrak{g}(N)=\exp\left[-\nu\int^N dm\left\{\frac{1}{\mathcal{F}_-(m)}+\frac{1}{\mathcal{F}_+(m)}\right\}\right]=\left[\frac{(N_+^*-N)(N-N_-^*)}{N^2}\right]^{\frac{\nu}{1+q}}, \tag{S7}$$

and $\mathcal{F}_\pm$ are defined by eq. (10). The *joint stationary PDF* giving the probability density of N in each environmental state is thus explicitly given by

$$p^*(N,\xi)=\frac{\mathcal{Z}}{\xi\mathcal{F}(N,\xi)}\,\mathfrak{g}(N)=\frac{\mathcal{Z}}{\xi\mathcal{F}(N,\xi)}\left[\frac{(N_+^*-N)(N-N_-^*)}{N^2}\right]^{\frac{\nu}{1+q}}, \tag{S8}$$

where $\mathcal{Z}$ is the normalization constant. In figure S1, we compare the predictions of the joint PDF $p^*(N,\xi)$ with the histograms of the population size obtained from SSA results, verifying that the PDMP description aptly reproduces the location and number of peaks that characterize the quasi-stationary distribution of N (see also [12, 13]).

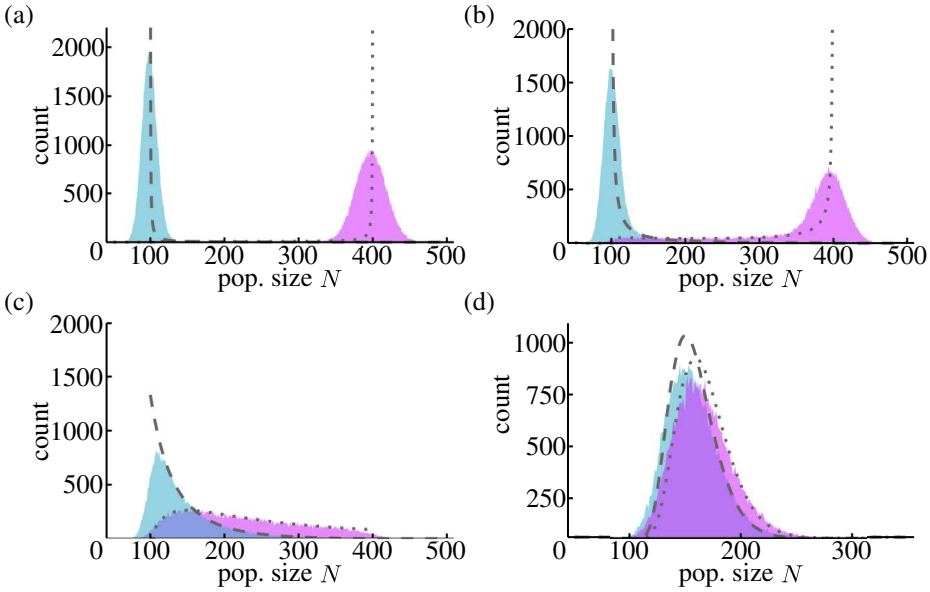

Figure S1: Histograms of population size (N-QSD) and from the joint PDMP PDF (S8) when $b=0$, for (a) $\nu=0.01$, (b) $\nu=0.1$, (c) $\nu=1$, and (d) $\nu=10$. Shaded areas correspond to SSA results for $\xi=+1$ (purple) and $\xi=-1$ (cyan); dashed and dotted lines are from (S8) with $\xi=+1$ and $\xi=-1$, respectively. Parameters are $(K_+,K_-,s,x_0,b)=(400,100,0.02,0.5,0)$

The marginal stationary PDF $p^*(N)=p^*(N,\xi)+p^*(N,-\xi)$ is thus $p^*(N)\propto[(1/\mathcal{F}_+(N))-(1/\mathcal{F}_-(N))]\,\mathfrak{g}(N)$, which yields the explicit expression (S3).

It is also useful to notice that, at stationarity, the probability that the PDMP (S2) is in the environmental state ξ, given a population size N is given by [11]

$$p^*(\xi|N)=\frac{-\xi\mathcal{F}(-\xi,N)}{\sum_{\xi=\pm1}\xi\mathcal{F}(\xi,N)}. \tag{S9}$$

4 Assessment of accuracy of formulas for the fixation probability

A central point of our analysis is the formula to compute the fixation probability of S (see section III.C.1 in the main text), ϕ, with the formula [12]

$$\phi \simeq \int_{K_-}^{K_+} \phi|_N \, p^*_{\nu/s}(N)\, dN = \mathcal{Z}_\nu \int_{K_-}^{K_+} \frac{e^{-Ns(1-x_0)} - e^{-Ns}}{N^2(1-e^{-Ns})} \left[\frac{(K_+ - N)(N - K_-)}{N^2}\right]^{\nu-1} dN, \qquad \text{(S10)}$$

when $b = 0$ (no public good production). As shown in figure S2(a,b), this formula correctly captures the nontrivial functional dependence of ϕ on ν and s, see also Ref. [12].

When $s = \mathcal{O}(1)$, the assumption of a timescale separation between N and x that underpins the derivation of equation (S10) is no longer valid. As a consequence, the relative deviations between the predictions of eq. (S10) and the SSA results for ϕ increase with s, as shown in figure S2(b,c). To quantify the accuracy of equation (S10), we have compared its predictions with the simulation results of 10^6 realizations obtained for different values of ν and s spanning between 0 and 0.25, recording the SSA fixation probability ϕ_{sim}. For each combination of parameters (different colors in Figure S2(b,c)), we determined the theoretical prediction ϕ_{th} from eq. (S10) and the percentage deviation between it and the simulation result $\Delta\phi = 100|\phi_{\text{th}} - \phi_{\text{sim}}|/\phi_{\text{sim}}$. As figure S2(b,c) shows, theoretical results reproduce simulations for small s, with relative deviations below 10%. Discrepancies increase more and more as the selection intensity is increased towards $s = \mathcal{O}(1)$ (when $s > 0.1$, in figure S2)(b,c). The approximation underpinning (S10) is therefore valid in the regime $s \ll 1$, which is the regime of weak selection pressure on which we focus (see main text), and deteriorates as s approaches $s = \mathcal{O}(1)$.

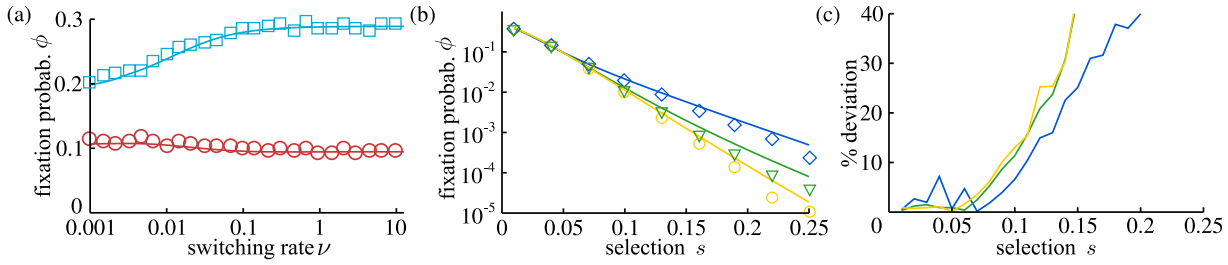

Figure S2: (a) ϕ vs. ν when $b = 0$, for $s = 0.02$ ($\square$, cyan) and $s = 0.05$ ($\circ$, red). (b) ϕ vs. s when $b = 0$, with $\nu = 0.1$ ($\circ$, yellow), $\nu = 1$ (∇, green), $\nu = 10$ ($\diamond$, blue). (c) Accuracy of formula as function of s with $b = 0$, measured as the relative deviations from simulation results for ϕ with the same ν as in (b), see text for details. In panels (a) and (b) symbols are from simulations (10^4 realizations in (a) and 10^6 runs in (b)) and solid lines are from formula (S10). Panel (c) has been obtained as explained in the text. Other parameters are $(K_+, K_-, x_0) = (450, 50, 0.5)$

Within the regime $s \ll 1$, we have similarly assessed the accuracy of equation (S10) for different switching rates ν. We simulated 10^4 realizations of the system, for different values of s, and 100 values ν between 0.001 and 10 and computed the percentage deviation $\Delta\phi(\nu)$ as explained above. Dots in figure S3(a) are thus based on ϕ_{sim} obtained by sampling 10^4 SSA realizations; they represent the value of $\Delta\phi(\nu)$ recorded at each value of ν, with different colors signaling different values of s (red for 0.05, cyan for 0.02). The dots scatter uniformly, indicating no systematic trend in the deviation. For $s = 0.02$, we observe deviations between 0 and 8% when $s = 0.02$, with an average (solid line) of 2% and standard deviation (shaded area) $\approx 2\%$; for $s = 0.05$ (red), deviations are between 0 and 13%, with average 4% and standard deviation 2.5%.

For the case with public good production, we have used an effective approach and obtained the following expression for the fixation probability of S (see section III.C.2 in the main text):

$$\phi_q = \int_{(1+q)K_-}^{(1+q)K_+} \phi|_N \, p^*_{\nu/s,q}(N)\, dN\,, \quad \text{when } b > 0 \text{ (public good production).} \qquad \text{(S11)}$$

This expression also builds on a timescale separation between an effective population size and x. Besides the breakdown of the timescale separation when $s = \mathcal{O}(1)$, the accuracy of the approximation $\phi \simeq \phi_q$ deteriorates for higher values of b and/or s, because the fixation of S then becomes increasingly unlikely, see figure 3(a), which limits the accuracy with which $q(b)$ is determined and hence the predictions of equation (S11).

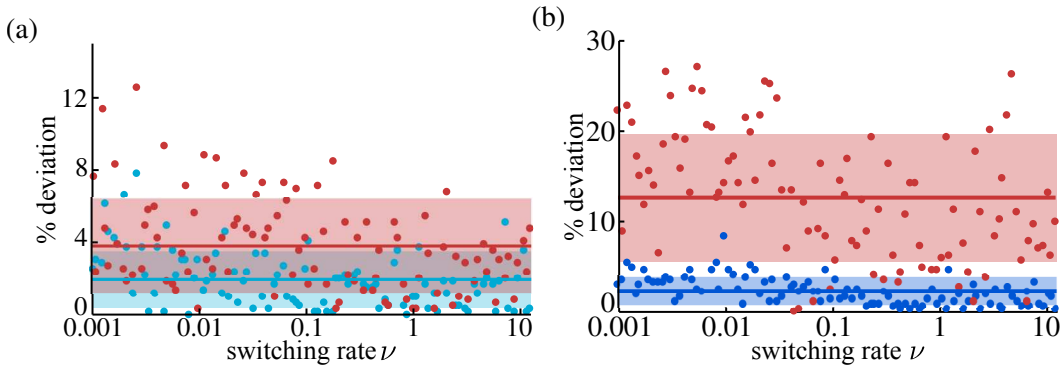

Figure S3: (a) Percentage deviation $\Delta\phi$ between simulation and theory vs. ν, for $b = 0$ with $s = 0.02$ (cyan) and $s = 0.05$ (red). Dots represent the percentage distance between prediction and simulated value for each ν, solid lines denote the average of the dots, shaded areas the standard deviation around the average. (b) Same as in panel (a) but for $(s, b) = (0.02, 0.2)$ (blue) and $(0.05, 2)$ (red). Other parameters are $(K_+, K_-, x_0) = (450, 50, 0.5)$.

Figure S3(b) shows the results for the percentage deviation of the predictions of equation (S11), using the appropriate values of the effective parameter $q(b)$ (excluding a few outliers), and $\phi_{\rm sim}$ obtained from 10^4 SSA realizations. For $s = 0.02$, $b = 0.2$ (blue), $\Delta\phi$ is between 0 and 8%, with average 3% and a standard deviation of 2%. For $s = 0.05$, $b = 2$ (red), we observe larger and more scattered $\Delta\phi$ between 0 and 28%, with average 12% and standard deviation 7%. While a deterioration of the approximation when s and b are increased can explain the increase in the average $\Delta\phi$, higher values of s and b also cause lower fixation probabilities for S, see figure 3(a). The corresponding values of ϕ are small which results in noisier values of $\phi_{\rm sim}$ and $\Delta\phi$, as shown by red data in figure S3.

Overall, the above analyis confirms that our approach is able to predict the fixation probability ϕ in the regime of weak selection intensity ($0 < s \ll 1$), both when $b = 0$ and $0 < b = \mathcal{O}(1)$, with a remarkable accuracy of a few percent over a vast range of values ν.

5 Fixation in the fitness-dependent Moran process & Mean fixation time under switching carrying capacity

5.1 Fixation in the fitness-dependent Moran process

To study the fixation properties of the system, we have used the properties of the fitness-dependent Moran Process (fdMP) outlined in section III.B of the main text [14, 15, 16, 17]. In a population of large but finite and constant size N, the fixation properties under weak selection of the fdMP can be inferred from the backward Fokker-Planck equation associated with the generator [18, 19, 20, 14, 15, 17]

$$\mathcal{G}(x)|_N = g(x)\,\frac{x(1-x)}{N}\left[-Ns\frac{d}{dx} + \frac{d^2}{dx^2}\right], \quad \text{where } g(x) = 1 + bx. \tag{S12}$$

For an initial fraction x_0 of S individuals, the fixation probability $\phi(x_0)|_N$ of S obeys $\mathcal{G}(x)|_N\phi(x)|_N = 0$, with $\phi(1)|_N = 1$ and $\phi(0)|_N = 0$ (absorbing boundaries at $x = 0, 1$). Yielding the result

$$\phi(x_0)|_N \;=\; \frac{e^{-Ns(1-x_0)} - e^{-Ns}}{1 - e^{-Ns}}, \tag{S13}$$

given as equation (12) in the main text.

The generator (S12) can also be used to study when fixation occurs in the fdMP in the realm of the diffusion approximation [14, 15, 17, 18]. Quantities of particular interest, are the unconditional mean fixation time (MFT)—which is the average time to reach any of the absorbing states, here either $x = 0$ or $x = 1$—as well as the conditional MFTs—the mean time to reach a specific absorbing boundary. The unconditional MFT is obtained by solving $\mathcal{G}(x_0)|_N\, T(x_0)|_N = -1$ subject to $T(0)|_N = T(1)|_N = 0$ [19, 14, 18]. The conditional MFT to reach $x = 1$ is denoted by $T^S(x_0)|_N$, while $T^F(x_0)|_N$ is the (conditional) MFT conditioned to reach $x = 0$. The MFTs and the

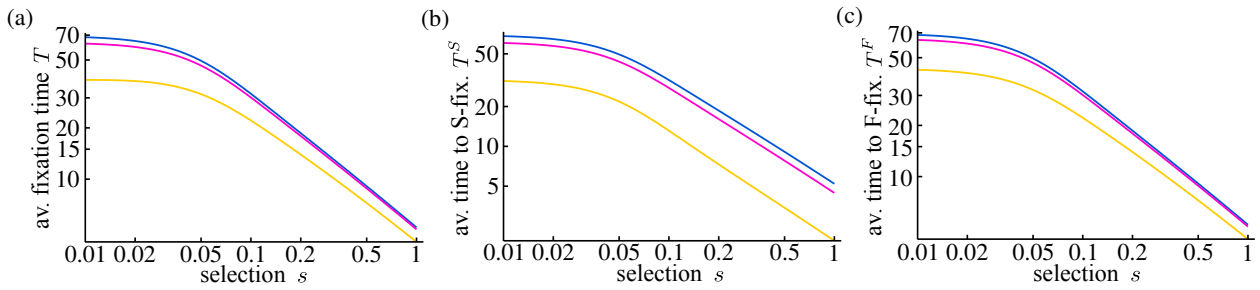

Figure S4: (a) MFT $T|_N$ vs. s for the fdMP, given by $T|_N = \phi|_N T^S|_N + (1-\phi|_N)T^F|_N$. In the case $b = 0$ (blue), this corresponds to equation (S15). (b) $T^S|_N$ vs. s for the fdMP, from the solution of the appropriate equation associated with the generator (S12). (c) $T^F|_N$ vs. s for the fdMP, obtained as T^S. The population in the fdMP is of constant size $N = 100$ and the effect of the public good parameter b is to reduce the relaxation time of x, and thus to lower all the MFTs with respect to the case $b = 0$. However, the MFTs always scale as $\mathcal{O}(1/s)$ to leading order when $s \ll 1$. In all panels, and $b = 0$ (blue), $b = 0.2$ (pink), $b = 2$ (yellow), $x_0 = 0.5$.

fixation probabilities are related by $T(x)|_N = \phi T^S(x_0)|_N + (1-\phi)T^F(x_0)|_N$. Explicit, but unwieldy, expressions for the MFTs in the fdMP can be obtained [19, 14, 18, 15], *e.g.* the unconditional MFT in the case $b = 0$ reads

$$\begin{aligned} T(1/2)|_N &= \frac{1}{s}\left\{(1-2\phi(1/2)|_N)(\ln(Ns)+\gamma) + \mathrm{e}^{-\frac{Ns}{2}}\mathrm{Ei}\left(\frac{Ns}{2}\right) - \mathrm{e}^{\frac{Ns}{2}}\mathrm{Ei}\left(-\frac{Ns}{2}\right)\right. \\ &+ \left. \mathrm{e}^{Ns}\phi(1/2)|_N\mathrm{Ei}(-Ns) - \mathrm{e}^{-Ns}(1-\phi(1/2)|_N)\mathrm{Ei}(Ns)\right\}, \end{aligned} \tag{S14}$$

where $\gamma \approx 0.577...$ is the Euler-Mascheroni constant, and $\mathrm{Ei}(z) = \int_{-z}^{\infty} dz \frac{e^{-z}}{z}$ is the exponential integral. Hence, in the regime where $s \ll 1$, with $Ns \gg 1$, and $s(\ln N) \ll 1$ (with x_0 is sufficiently separated from $x = 0, 1$), $T(x_0)|_N \sim (\ln N)/s$ [14, 15, 17], with a subleading prefactor $\sim \ln N$. The conditional MFTs exhibit the same behavior $T^{S/F}(x_0) \sim T(x_0) = \mathcal{O}(1/s)$ to leading order when $s \ll 1$, see figure S4. A similar behavior also holds when $b > 0$ and $s \ll 1$, with a subleading prefactor that then depends (weakly) on the public good parameter $b = \mathcal{O}(1)$, specifically $T(x_0)|_N \sim (\ln(N - \mathcal{O}(b)))/s$, as confirmed by figure S4. The public good parameter b, in fact, reduces the relaxation time of x, see equation (7), which results in a weak reduction of the unconditional and MFTs with respect to the case with $b = 0$, see also figure S4(b,c). The most relevant point for our purposes, is the fact that the unconditional MFT of the fdMP scales as $\mathcal{O}(1/s)$ to leading order when $s \ll 1$ when $Ns \gg 1$, and so do the conditional MFTs, in both cases $b = 0$ and $b > 0$.

Results (S12)-(S14) can be used to obtain the fixation properties of fdMP in a population of finite size subject to a *constant* carrying capacity K. This is done by setting $N = K$ in (S12)-(S14), which neglects the rare/unlikely early fixation events occurring during the exponential (growth) phase.

5.2 Mean fixation times with a switching carrying capacity

In a population subject to a randomly switching carrying capacity, with no public good production, the size and growth rate are independent of the composition. As explained in Ref. [12, 13], when $b = 0$, the conditional and unconditional MFTs admit the same scaling to leading order when $s \ll 1$, i.e. $T^{S/F}(x_0) \sim T(x_0) = \mathcal{O}(1/s)$, and we can use the approach outlined in Section III.C.1, to compute [13]

$$T(x_0) \simeq \int_{K_-}^{K_+} T(x_0)|_N p^*_{\nu/s}(N)\, dN. \tag{S15}$$

Figure S5(a) shows that the predictions of this formula (blue line) agree extremely well with SSA results ($\diamond$). This confirms that under weak selection and $b = 0$, the unconditional MFT scales as in the fdMP, i.e. $T(x_0) = \mathcal{O}(1/s)$ when $s \ll 1$ and $\langle K\rangle s \gg 1$. This implies that after $t \gtrsim 1/s$ fixation is likely to have occurred, and that the population size is at quasi-stationarity when $t \gg 1/s$. Quite remarkably, we also notice in figure S5(a) that even when $s = \mathcal{O}(1)$ there is a good agreement between the predictions of eq. (S15) and SSA results.

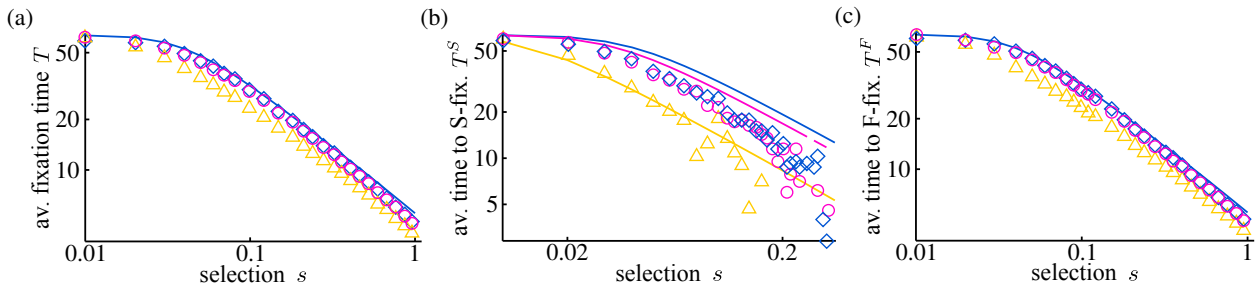

Figure S5: (a) MFT T vs s. Symbols are from simulations (10^4 realizations) and the solid line shows $T(x_0)$ given by eq. (S15) in the case $b = 0$. (b) T^S vs s. Solid lines are the results of equation (S16) . (c) T^F vs s. The solid line is the result of equation (S17). In all panels, $\nu = 0.1$ and $b = 0$ (blue, $\diamond$), $b = 0.2$ (pink, $\circ$), $b = 2$ (yellow, $\triangle$), other parameters are $(K_-, K_+, x_0) = (50, 450, 0.5)$.

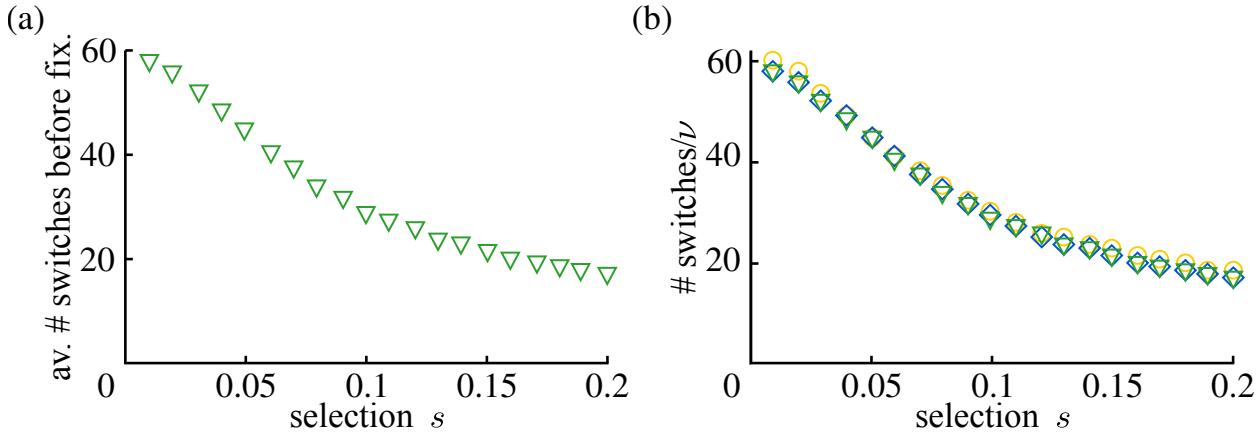

Figure S6: (a) Average number of switches prior to fixation vs. s for $\nu = 1$ is shown to be of order $\mathcal{O}(\nu/s)$ when $s \ll 1$ and $\langle K \rangle s \gg 1$. (b) Average number of switches prior to fixation rescaled by a factor $1/\nu$ vs. s for $\nu = 0.1$ (circles), $\nu = 1$ (downside triangles) and $\nu = 10$ (diamonds). In both panels, simulation results are averaged over 10^4 realizations. Parameters are $(K_+, K_-, b) = (450, 50, 0)$. In panel (b), the different symbols essentially collapse onto a single curve showing that, on average, the number of switches prior to fixation increase linearly with ν and mostly independent of the population size, see text.

In the case $b > 0$, the evolution of the population size and its composition are coupled. As discussed in the main text, S is less likely to fixate when b is increased, and the population size at fixation depends on which species takes over (the population size is typically larger when S fixates). On the other hand, according to eq. (7), increasing b reduces the relaxation time of x. Since these two effects balance each other, we expect the effect of $b > 0$ to be even weaker in the switching environment than in the fdMP with constant population size. Having seen that b has a weak effect on the MFTs, we anticipate that the MFTs with a switching carrying capacity exhibit a similar behavior as those of the fdMP. To verify this picture and figure out on which timescale fixation occurs when $b > 0$, we have considered the fixation of S and F separately by studying their conditional MFTs [13]. For this, we can attempt to generalize the approach used in the case $b = 0$ and consider the averages over the conditional stationary PDFs $p^*_{\nu/s,b}(N)$ and

$p^*_{\nu/s}(N)$ obtained from (S3) with $q = b$ and $q = 0$, i.e.

$$T^S(x_0) \simeq \int_{(1+b)K_-}^{(1+b)K_+} T^S(x_0)|_N p^*_{\nu/s,b}(N)dN\,, \tag{S16}$$

$$T^F(x_0) \simeq \int_{K_-}^{K_+} T^F(x_0)|_N p^*_{\nu/s}(N)dN\,, \tag{S17}$$

$$T(x_0) \simeq \phi_{q(b)}T^S(x_0) + (1-\phi_{q(b)})T^F(x_0)\,, \tag{S18}$$

where $T^{S/F}(x_0)|_N$ are the conditional MFTs of the fdMP with $b > 0$. A clear limitation of formula (S16) and (S17) stems from the fact that $p^*_{\nu/s,b}(N)$ and $p^*_{\nu/s}(N)$ provide a good approximation of the N-QSD in the quasi-stationary state that is reached after $t \gg 1/s$, see Ref. [21], i.e. well after fixation has typically occurred. However, since the population size and the parameter b only yield subleading contributions to the MFTs of the fdMP when $s \ll 1$, we expect that formula (S16)-(S18) are still able to capture how the MFTs scale to leading order under weak selection intensity. The comparison of SSA results for the MFTs with $b > 0$ reported in figure S5, and their comparison with those of figure (S4) confirm this picture. Since the b-dependence of the MFTs in figure (S4) is clearly subleading, we can simplify the evaluation of (S16) by setting $g \equiv 1 + b$ (and similarly $g \equiv 1$ in (S17)). As shown in figure (S5)(b), this does not affect the leading behavior of T^S.

Figures S5(b,c) show that the simplified formula (S16) and (S17) indeed correctly predict that the conditional MFTs scale as $\mathcal{O}(1/s)$ when $s \ll 1$ and $\langle K\rangle s \gg 1$, even if, as expected, they overstimate the SSA results for T^S and T^F. Hence, equation (S18) predicts that to leading order the unconditional MFT scales as $\mathcal{O}(1/s)$, which is in good agreement with the SSA results reported in figure S5(a). As s and b increase, the fixation of S becomes less likely and thus $T(x_0) \simeq T^F(x_0)$, as shown by figures S5(a) and (c). We notice that SSA results reported in figure S5 confirm that the MFTs with randomly switching carrying capacity depend even more weakly on the public good parameter b than in the fdMP where N is constant.

We therefore conclude that, under weak selection $1/\langle K\rangle \ll s \ll 1$, and with $b = \mathcal{O}(1)$, the MFTs in the case $b > 0$ scale as $\mathcal{O}(1/s)$. This means that the fixation in the public good scenario ($b > 0$) is likely to have occurred when $t \gtrsim 1/s$, as in the case $b = 0$. This also implies that, when $b \geq 0$, the population size is most probably at quasi-stationarity when $t \gg 1/s$, and its composition consists then of only F or S individuals. These results thus indicate that, to leading order in $1/s$ (with $\langle K\rangle s \gg 1$), the MFTs here scale as in the absence of external noise. Hence, while environmental noise has a significant effect on the fixation probability (see Section III.C in the main text), its effect on the MFTs is much less important, as captured by the formula (S16)-(S18). A consequence of these results is that the population experiences, on average, $\mathcal{O}(\nu/s)$ switches prior to fixation when $b \geq 0$ and $1/\langle K\rangle \ll s \ll 1$. In fact, the figure S6 confirms that the average number of switches prior to fixation scales as $1/s$ to leading order when $1/\langle K\rangle \ll s \ll 1$ in the case $b = 0$. In figure S6(b), we show that the average number of switches prior to fixation increases linearly with ν, with simulation data for different values of ν essentially collapsing when rescaled by a factor $1/\nu$. Since the population size greatly varies when ν changes, see, *e.g.* the videos in [21], the fact that the average number of switches increases simply linearly with ν is a strong indication of its weak dependence on the population size, and is a further argument supporting the rescaling $\nu \to \nu/s$ in formula (S10) and (S11).

6 Supplementary information on the PDMP approximation and the "Eco-evolutionary game"

6.1 PDMP approximation and average number of individuals

The analysis of the correlations between population size and its composition (Section IV.A), and that of the "eco-evolutionary game" (Section IV.B), relies largely on properties of the average population size at quasi-stationarity given by

$$\langle N\rangle^*_{\nu,b} = \phi_b\langle N\rangle^*_{\nu,b} + (1-\phi_b)\langle N\rangle^*_{\nu,0} = (1+b)\phi_b\langle N\rangle^*_{\frac{\nu}{1+b},0} + (1-\phi_b)\langle N\rangle^*_{\nu,0}\,, \tag{S19}$$

where ϕ_b is the fixation probability of species S under a public good parameter b, within what in the main text is referred to as the "PDMP approximation". This approximation consists of averaging the population size N over the marginal PDF (S3) of the PDMP (S2).

To derive equation (S19), which coincides with equation (16) of the main text, we first notice that $\langle N\rangle^*_{\nu,b}$ consists of the average population size conditioned to the fixation of F and S, i.e. $\langle N\rangle^*_{\nu,b} = \langle N_F\rangle^*_{\nu,b} + \langle N_S\rangle^*_{\nu,b}$. The fixation

of F occurs with probability $\widetilde{\phi}_b = 1 - \phi_b$, and results in a global growth rate $g = 1$, yielding

$$\langle N_F \rangle^*_{\nu,b} = \langle N | x = 0 \rangle^*_{\nu,b} = \widetilde{\phi}_b \langle N \rangle^*_{\nu,0} = \widetilde{\phi}_b \int_{K_-}^{K_+} N p^*_\nu(N) dN, \tag{S20}$$

where $\langle N \rangle^*_{\nu,0}$ is the quasi-stationary average population size when $b = 0$ and the integration is over $p^*_\nu \equiv p^*_{\nu,0}$ given by eq. (S3). Similarly, the fixation of S occurs with probability ϕ_b, after which $g = 1 + b$, yielding

$$\langle N_S \rangle^*_{\nu,b} = \langle N | x = 1 \rangle^*_{\nu,b} = \phi_b \langle N \rangle^*_{\nu,b} = \phi_b \int_{(1+b)K_-}^{(1+b)K_+} N p^*_{\nu,b}(N) dN = (1+b)\phi_b \langle N \rangle^*_{\frac{\nu}{1+b},0}. \tag{S21}$$

The last equality is obtained by performing the change of variable $N \to N/(1+b)$ and allows us to express $\langle N \rangle^*_{\nu,b}$ in terms of the average when $b = 0$. Putting everything together, we obtain equation (S19):

$$\begin{aligned} \langle N \rangle^*_{\nu,b} &= (1+b)\phi_b \langle N \rangle^*_{\frac{\nu}{1+b},0} + (1-\phi_b)\langle N \rangle^*_{\nu,0} \\ &\simeq (1+b)\phi_{q(b)} \int_{K_-}^{K_+} N p^*_{\frac{\nu}{1+b}}(N)\, dN + (1-\phi_{q(b)}) \int_{K_-}^{K_+} N p^*_\nu(N)\, dN, \end{aligned} \tag{S22}$$

where in the last line we have used the approximation $\phi_b \simeq \phi_{q(b)}$ given by equation (S11). Figure 3(b) shows that predictions of $\langle N \rangle^*_{\nu,b}$ obtained with this approach are as close to simulation results as their counterparts obtained by averaging over the PDF obtained within the linear noise approximation of Section V (see also Section 7 below). It is clear from (S11) that $\langle N \rangle^*_{\nu,b}$ is an increasing function of b since $\langle N \rangle^*_{\nu,0}$ is a decreasing function of ν [‡].

In Section IV, we have often considered the limiting regimes of very fast/slow switching, $\nu \to \infty, 0$, in which the analytical formula greatly simplify. To obtain these simplified expressions, it suffices to notice that

$$\int_{K_-}^{K_+} N p^*_\nu(N) dN = \begin{cases} \mathcal{K} & \text{when } \nu \to \infty \\ \langle K \rangle & \text{when } \nu \to 0 \end{cases}$$

Hence, when $\nu \gg 1$, we have $\langle N_F \rangle^*_{\nu,b} \to (1-\phi_b)\mathcal{K}$ and $\langle N_S \rangle^*_{\nu,b} \to (1+b)\phi_b \mathcal{K}$. Similarly, when $\nu \ll s$, we have $\langle N_F \rangle^*_{\nu,b} \to (1-\phi_b)\langle K \rangle$ and $\langle N_S \rangle^*_{\nu,b} \to (1+b)\phi_b \langle K \rangle$. Hence, from (S22) and using $\phi \simeq \phi_{q(b)}$ we obtain the average population size in the limiting regimes:

$$\langle N \rangle^*_{\nu,b} = \begin{cases} \left[1 + b\phi^{(\infty)}_{q(b)}\right] \mathcal{K} & \text{when } \nu \to \infty \\ \left[1 + b\phi^{(0)}_{q(b)}\right] \langle K \rangle & \text{when } \nu \to 0. \end{cases} \tag{S23}$$

The limiting behavior reported as dashed lines in figures 3(b) and 4(b) can readily be obtained from equations (S23).

6.2 Best conditions for cooperation in the eco-evolutionary game

A finite well-mixed population of constant size is the natural setting of evolutionary game theory (EGT). The notion of evolutionary stability is central to EGT since an evolutionary stable strategy, when adopted by a population, cannot be invaded and replaced by an alternative strategy. For a population with two possible strategies, one is evolutionary stable if it satisfies the so-called invasion and replacement conditions [22, 23]. As a result, the sole fact that one strategy has a higher fitness than another does not guarantee that it is evolutionary stable since an individual of the other type may have a better chance to fixate the population.

For the model considered here, in a finite and static population, the strain F has always a higher fitness than S, and the fixation probability of S vanishes exponentially with the population size, see equation (S13). In a finite and static population, F is therefore evolutionary stable, and in this sense always superior to S.

The situation is radically different in the eco-evolutionary game considered here since the population continues to evolve in a *fluctuating environment* even after fixation, and the notions of non-invadibility / non-replacement are no longer suitable to measure the species evolutionary success:

[‡] With eq. (S3), in the realm of the PDMP approximation, we find that $(1 + b\phi_b)\langle N \rangle^*_{0,\nu} \leq \langle N \rangle^*_{b,\nu} \leq (1 + b\phi_b)\langle K \rangle$.

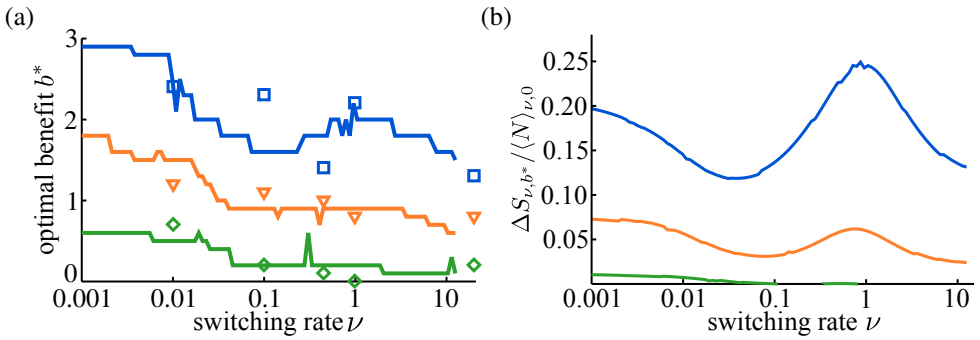

Figure S7: (a) Optimal public good benefit parameter for the cooperating b^* vs ν for $s = 0.02$ (blue), $s = 0.03$ (orange), and $s = 0.05$ (green). Symbols are results from simulations and solid lines are from (25) (b) $\Delta S_{\nu,b^*}/\langle N\rangle^*_{\nu,0}$ vs. ν, obtained gives the highest payoff received by S by producing the public good at optimal value $b = b^*(\nu, s)$ obtained from (25) for $s = 0.02$ (blue), $s = 0.03$ (orange), $s = 0.05$ (green), see below and main text. Other parameters are $(K_+, K_-, x_0) = (450, 50, 0.5)$.

As discussed in Section IV.B of the main text, even if S has always a lower fitness and a lesser chance to fixate than F, its occasional fixation can prove very rewarding since it allows cooperators to establish a large community of S individuals (of a size that can be significantly larger than the size of an average community of F individuals). In the context of the interpretation of the eco-evolutionary game in terms of a biologically motivated metapopulation of non-interacting communities, see Section IV.B of the main text, we have proposed to measure the success of S and F in this eco-evolutionary game by computing the difference between the expected long-term number of individuals $\Delta S_{\nu,b}$ and $\Delta F_{\nu,b}$, compared to the $b = 0$ case. $\Delta S_{\nu,b}$ and $\Delta F_{\nu,b}$ thus serve as expected payoffs in our eco-evolutionary game. In the PDMP approximation, we can use our effective approach (see section III.C.2) and equations (S20) and (S21), to obtain

$$\Delta S_{\nu,b} = (1+b)\phi_{q(b)} \int_{K_-}^{K_+} N p^*_{\frac{\nu}{1+b}}(N)\, dN - \phi_0 \int_{K_-}^{K_+} N p^*_{\nu}(N)\, dN \tag{S24}$$

$$\Delta F_{\nu,b} = (\phi_0 - \phi_{q(b)}) \int_{K_-}^{K_+} N p^*_{\nu}(N)\, dN\,, \tag{S25}$$

where $p^*_\nu(N)$ is readily obtained by setting $q = 0$ in equation (S3). In the limiting regimes $\nu \to \infty, 0$, with (S23), we obtain

$$\Delta S_{\nu,b} = \begin{cases} \left[(1+b)\phi^{(\infty)}_{q(b)} - \phi^{(\infty)}_0\right] \mathcal{K} & \text{when } \nu \to \infty \\ \left[(1+b)\phi^{(0)}_{q(b)} - \phi^{(0)}_0\right] \langle K\rangle & \text{when } \nu \to 0. \end{cases} \quad \text{and} \quad \Delta F_{\nu,b} = \begin{cases} \left[\phi^{(\infty)}_0 - \phi^{(\infty)}_{q(b)}\right] \mathcal{K} & \text{when } \nu \to \infty \\ \left[\phi^{(0)}_0 - \phi^{(0)}_{q(b)}\right] \langle K\rangle & \text{when } \nu \to 0. \end{cases} \tag{S26}$$

As shown in figure 5, $\Delta S_{\nu,b}$ is non-monotonic in b and has a maximum for $b = b^*$. This is then the optimal value of b for the cooperating strain S (given s, ν, $K_\pm$). Figure S7(a) shows the dependence of the optimal value $b^* = b^*(\nu, s)$ on ν, for different intensities of the selection pressure s. Clearly, $b^* = b^*(\nu, s)$ exhibits a complex, non-monotonic, dependence on ν and decreases when s increases, in a similar fashion to b_c (see main text). In figure S7(a), symbols are from simulations and the lines have been obtained from evaluating the maximum of equation (S24).

Figure S7(b) shows $\Delta S_{\nu,b^*}/\langle N\rangle^*_{\nu,0}$: the optimal payoff for cooperators divided by the long-time average population at $b = 0$. In other words, it shows how much bigger is, on average, the best-performing cooperating population, compared to the average population at $b = 0$. For sufficiently low s, e.g. for $s = 0.02$ (blue), the public good can make the average number of S individuals be up to $12\% - 25\%$ larger than the average population at $b = 0$ ($\Delta S_{\nu,b^*}/\langle N\rangle^*_{\nu,0} \approx 0.12 - 0.25$ across all values of ν). Figure S7(b) corresponds to results at quasi-stationarity, i.e. after fixation has occurred (with a smaller probability for S than F) and therefore shows the actual long-term eco-evolutionary payoff for cooperation: In the optimal conditions, the S strain can gain a significant benefit from the production of a public good.

As discussed in Section IV.B of the main text, there are conditions under which S receives a higher expected payoff than F in the sense that $\Delta S_{\nu,b} > \Delta F_{\nu,b}$. When this happens, cooperating is not only beneficial but is also advantageous for S. We have considered that for given parameters (ν, s), it is best to cooperate for the production of a public good with benefit parameter b when the following two conditions are satisfied: (a) $\Delta S_{\nu,b} > \Delta F_{\nu,b}$; (b) $b = b^*(\nu, s) < \beta(\nu, s)$. These conditions ensure (a) that S receives a higher payoff than F, and (b) that S receives the maximum payoff under the switching rate ν and selection strength s. On the other hand, species F always outperforms S when $b > \beta(\nu, s)$ since it then receives a higher expected payoff than S, with $\Delta F_{\nu,b}$ that is an increasing function of b for all values of ν and s, see figure 5(c).

As shown in figure 6(b) the phases (ii), ($0 < \Delta S_{\nu,b} < \Delta F_{\nu,b}$) and (iii) ($\Delta S_{\nu,b} > \Delta F_{\nu,b}$) are separated by the value $b = \beta(\nu, s)$ at which $\Delta S_{\nu,\beta} = \Delta F_{\nu,\beta}$, defined as by the solution of

$$\frac{1}{1+\beta}\left(\frac{2\phi_0}{\phi_{q(\beta)}} - 1\right) = \frac{\int_{K_-}^{K_+} N p^*_{\frac{\nu}{1+\beta}}\, dN}{\int_{K_-}^{K_+} N p^*_{\nu}\, dN}\,. \tag{S27}$$

It is noteworthy that in the limiting switching regimes $\nu \gg 1$ and $\nu \ll s$, this equation greatly simplifies. In fact, using (S23), equation (S27) becomes $(1+\beta/2)\phi^{(\infty,0)}_{q(\beta)} = \phi^{(\infty,0)}_0$ when $\nu \gg 1$ and $\nu \ll s$, respectively. Hence, the corresponding payoffs along $b = \beta(\nu, s)$ are $\Delta S_{\nu,\beta} = \Delta F_{\nu,\beta} = (\phi^{(\infty)}_0 - \phi^{(\infty)}_\beta)\mathcal{K} \simeq \beta\phi^{(\infty)}_{q(\beta)}\mathcal{K}/2$ when $\nu \gg 1$ and $\Delta S_{\nu,\beta} = \Delta F_{\nu,\beta} \simeq \beta\phi^{(0)}_{q(\beta)}\langle K\rangle/2$ when $\nu \ll s$, yielding $\Delta S_{\nu,\beta}/\langle N\rangle^*_{\nu,0} = \Delta F_{\nu,\beta}/\langle N\rangle^*_{\nu,0} \simeq \beta\phi^{(\infty,0)}_{q(\beta)}/2$ in both limiting regimes. It is however important to remember that in general $\phi_\beta \simeq \phi_{q(\beta)}$ depends nontrivially on ν and s, and can be either an increasing or decreasing function of ν, see figures 2(a) and 3(a).

While the choice made here on how to measure the success of S and F is arguably the most natural, we could have also considered other variants. For instance, we could have considered that the best conditions to cooperate for the production of the public good would be: S should receive a higher payoff than F, condition (a) as above, and, S should maximize the difference of payoffs $\Delta S_{\nu,b} - \Delta F_{\nu,b}$ (instead of condition (b)). This would lead to an optimal value of the public good benefit $\widetilde{b}$ that would generally differ from b^* especially at low switching rate (see figure 5(c)). While this alternative definition of the optimal payoff for S would lead to quantitative differences with the results reported in figure 6(b), the main qualitative features discussed here and in section IV.B would remain the same.

7 Effect of internal and environmental noise on population size distribution – Linear noise approximation about the PDMP predictions

The PDMP approximation of the N-QSD can reproduce the number and location of its peaks, but fails to capture the width of the distribution about the peaks and its accurate skewness, see, *e.g.*, figure S1. In this section, we derive the linear noise approximation (LNA) of the N-QSD used in Section V to account for the demographic fluctuations about the PDMP predictions [11].

After the fixation of species S, $N_S = N$ and $N_F = 0$, and the transition rates of the underpinning birth-death process become $T^+_S = (1+b)N$, $T^-_S = N^2/K(t)$, and $T^\pm_F = 0$. Similarly, after species F's fixation, $N_F = N$ and $N_S = 0$, and the transition rates (3) become $T^+_F = N$, $T^-_F = N^2/K(t)$, with $T^\pm_S = 0$. To deal simultaneously with the ecological dynamics arising after the fixation of either species, it is convenient to define the auxiliary stochastic logistic process $N \xrightarrow{T^+} N+1$ and $N \xrightarrow{T^-} N-1$, with symmetric dichotomous Markov noise $\xi(t) \in \{-1, +1\}$ and randomly switching carrying capacity defined by equations (3) and (4). This stochastic process is defined by the transition rates:

$$T^+ = (1+q)N,\;\; T^- = \frac{N^2}{K(t)} = N^2\left[\frac{1}{\mathcal{K}} - \xi(t)\left(\frac{1}{\mathcal{K}} - \frac{1}{K_+}\right)\right],\;\; \text{with}\;\; q = \begin{cases} b & \text{after fixation of } S \\ 0 & \text{after fixation of } F. \end{cases} \tag{S28}$$

As explained in section V.B of the main text, it is convenient to work with the continuous Markov process $\{n \equiv N/\Omega, \xi\}$ defined by

$$n \xrightarrow{\mathcal{T}^+} n + \Omega^{-1}, \quad n \xrightarrow{\mathcal{T}^-} n - \Omega^{-1}, \quad \text{with } \xi \xrightarrow{\nu} -\xi, \tag{S29}$$

with $\Omega = \langle K \rangle$ [§] and

$$\psi \equiv \lim_{\Omega\to\infty} N/\Omega, \quad \kappa \equiv \mathcal{K}/\Omega \quad \text{and} \qquad k_\xi \equiv \begin{cases} k_+ = K_+/\Omega & \text{if } \xi = 1 \\ k_- = K_-/\Omega & \text{if } \xi = -1. \end{cases}$$

Therefore, the transition rates for the process $\{n, \xi\}$ are

$$\mathcal{T}^+(\psi, \xi) = (1 + q)\psi \quad \text{and} \quad \mathcal{T}^-(\psi, \xi) = \psi^2 \left\{\kappa^{-1} - \xi(\kappa^{-1} - k_+^{-1})\right\}. \tag{S30}$$

It is also useful to define v_ξ, associated with the deterministic flows of $\{n, \xi\}$, and u_ξ associated with the diffusive flows:

$$v_\xi(\psi) \equiv \mathcal{T}^+ - \mathcal{T}^- = \frac{\mathcal{F}(\Omega\psi, \xi)}{\Omega} = \frac{\psi}{k_\xi}\left(\psi_\xi^* - \psi\right), \quad \text{and} \quad u_\xi(\psi) \equiv \mathcal{T}^+ + \mathcal{T}^- = \frac{\psi}{k_\xi}\left(\psi_\xi^* + \psi\right), \tag{S31}$$

with $\psi_\xi^* = (1 + q)k_\xi$. It is worth noting that $v_\xi(\psi) > 0$ when $\xi = +1$ and $v_\xi(\psi) < 0$ when $\xi = -1$.

When the environment is static ($K_\pm = K$), with $k_\xi = k$, $v_\xi = v$ and $u_\xi = u$, the LNA consists of performing a van Kampen system size expansion of the underlying master equation, which yields the Fokker-Planck equation (FPE) for the probability density $\pi(\eta, t)$ [20, 19]:

$$\partial_t \pi(\eta, t) = -\partial_\eta \left[\eta v'(\psi)\pi(\eta, t)\right] + \frac{u}{2}\partial_\eta^2 \pi(\eta, t), \tag{S32}$$

where $v' = dv/d\psi$ and $\pi(\eta, t)$ is the PDF of the fluctuations $\{\eta(t)\}$ about the mean-field trajectory $\dot{\psi} = v(\psi)$.

Here, the environment varies stochastically by randomly switching between two states and we are interested in the weak fluctuations about the PDMP trajectory $\psi(t)$. The process $\{n, \xi\}$ is thus analyzed in terms of a "pseudo-Fokker-Planck equation" which consists of an FPE, accounting for the internal noise, supplemented by terms arising from environmental stochasticity via the PDMP $\{\psi(t)\}$ defined by the stochastic differential equation

$$\dot{\psi} = v_\xi(\psi), \tag{S33}$$

that is equivalent to (S2) and whose joint PDF is readily obtained from (S8): $\pi^*_{\nu,q}(\psi, \xi) = \Omega p^*(\Omega\psi, \xi)$. Within the LNA, to account for the weak fluctuations about ψ up to linear order in η, we obtain the following pseudo-FPE for the PDF $\pi_{\nu,q}(\psi, \eta, \xi, t) \equiv \pi(\psi, \eta, \xi)$ of the process (S1):

$$\begin{aligned} \partial_t \pi(\psi, \eta, \xi) &= -\partial_\eta \left[\eta v'_\xi(\psi)\pi(\psi, \eta, \xi)\right] + \frac{u_\xi}{2}\partial_\eta^2 \pi(\psi, \eta, \xi) \\ &- \partial_\psi \left[v_\xi(\psi)\pi(\psi, \eta, \xi)\right] - \nu\left[\pi(\psi, \eta, \xi) - \pi(\psi, \eta, -\xi)\right], \end{aligned} \tag{S34}$$

where, for notational simplicity, in this section we drop the time dependence and the ν, q subscripts in the PDFs by writing $\pi(\eta, \xi)$ and $\pi(\psi, \eta, \xi)$ instead of $\pi_{\nu,q}(\eta, \xi, t)$ and $\pi_q(\psi, \eta, \xi, t)$, etc. On the RHS of eq. (S34), the first line corresponds to a usual FPE with a drift term $-\partial_\eta [\dots]$ and a diffusion coefficient u_ξ, while in the second line one recognizes the Liouvillian contribution $-\partial_\psi [v_\xi(\psi)\pi(\psi, \eta, \xi)]$ and terms from random switching.

To determine the stationary Gaussian probability density $\pi^*(\eta|\psi, \xi)$ characterizing the demographic fluctuations η about $\psi(t)$, we notice that $\pi(\psi, \eta, \xi) = \pi(\eta|\psi, \xi)\pi(\psi, \xi)$. As explained in the main text, we then assume that demographic fluctuations about ψ are the same in each environmental state $\xi = \pm 1$, and write $\pi(\eta|\psi, \xi) = \pi(\eta|\psi)$ [11]. With this assumption, we can set $\partial_t(\pi^*(\eta, \psi, \xi) + \pi^*(\eta, \psi, -\xi)) = 0$ and use equation (S34) to obtain

$$0 = -\left[\pi^*(\xi|\psi)v'_\xi(\psi) + \pi^*(-\xi|\psi)v'_{-\xi}(\psi)\right]\partial_\eta\left[\eta\pi^*(\eta|\psi)\right] + \frac{1}{2}\left[\pi^*(\xi|\psi)u_\xi(\psi) + \pi^*(-\xi|\psi)u_{-\xi}(\psi)\right]\partial_\eta^2\pi^*(\eta|\psi), \tag{S35}$$

where we have also used $\pi^*(\psi, \xi) = \pi^*(\psi)\pi^*(\xi|\psi)$ and the zero-current boundary condition $\sum_\xi v_\xi \pi^*(\psi, \xi) = 0$. At the PDMP level, equation (S9) expresses the probability of being in the environmental state ξ given that the population has size N. Hence, upon substituting $\pi^*(\xi|\psi) = -\xi v_{-\xi}/(\sum_{\xi=\pm1} \xi v_\xi)$, equation (S35) yields the stationary probability density $\pi^*(\eta|\psi)$ of an Ornstein-Uhlenbeck process [19, 20]. In other words, $\pi^*(\eta|\psi)$ is a Gaussian with zero mean and variance

$$\frac{u_-(\psi)v_+(\psi) - u_+(\psi)v_-(\psi)}{v_-(\psi)v'_+(\psi) - v_+(\psi)v'_-(\psi)} = \psi, \tag{S36}$$

[§] Since $K_\pm$ are here assumed to be of the same order, with $K_+ \gtrsim K_- \gg 1$, we could also define $\Omega = K_+$ or $\Omega = K_-$ and proceed similarly.

where we have used equation (S31), and the subscripts $\pm$ refer to $\xi = \pm 1$. With equation (S36), we find the stationary Gaussian probability density of the fluctuations about ψ:

$$\pi^*(\eta|\psi) = \frac{e^{-\frac{\eta^2}{2\psi}}}{\sqrt{2\pi\psi}}. \tag{S37}$$

Within the LNA, see eq. (25), the marginal quasi-stationary PDF of the process $\{N(t), \xi(t)\}$ defined by (S28) therefore is

$$p^*_{\mathrm{LNA},\nu,q}(N) = \frac{\pi^*(n)}{\Omega} = \sum_{\xi=\pm 1} \int\int d\psi d\eta \; \pi^*(\eta|\psi)\pi^*(\psi,\xi)\; \delta\left(n - \psi - \frac{\eta}{\sqrt{\Omega}}\right). \tag{S38}$$

Upon substituting (S37) and $\pi^*(\psi,\xi) = \Omega p^*_{\nu,q}(\Omega\psi,\xi)$ obtained from (S8), into (S38), we obtain the LNA-PDF of the process $\{N(t), \xi(t)\}$. When $b = 0$, the marginal LNA-PDF $p^*_{\mathrm{LNA},0}(N)$ in the case of the pure resource competition is obtained from $\pi^*(n)$ with $q = 0$ and reads

$$\begin{aligned} p^*_{\mathrm{LNA},\nu,0}(N) \quad \propto \quad & \int \frac{d\eta\; e^{-\eta^2/[2(n-\eta/\sqrt{\Omega})]}}{\left(n-\frac{\eta}{\sqrt{\Omega}}\right)^{3/2}\left(k_+ - \left(n-\frac{\eta}{\sqrt{\Omega}}\right)\right)} \left[\frac{\left\{k_+ - \left(n-\frac{\eta}{\sqrt{\Omega}}\right)\right\}\left\{\left(n-\frac{\eta}{\sqrt{\Omega}}\right) - k_-\right\}}{\left(n-\frac{\eta}{\sqrt{\Omega}}\right)^2}\right]^{\nu} \\ + \quad & \int \frac{d\eta\; e^{-\eta^2/[2(n-\eta/\sqrt{\Omega})]}}{\left(n-\frac{\eta}{\sqrt{\Omega}}\right)^{3/2}\left(\left(n-\frac{\eta}{\sqrt{\Omega}}\right) - k_-\right)} \left[\frac{\left\{k_+ - \left(n-\frac{\eta}{\sqrt{\Omega}}\right)\right\}\left\{\left(n-\frac{\eta}{\sqrt{\Omega}}\right) - k_-\right\}}{\left(n-\frac{\eta}{\sqrt{\Omega}}\right)^2}\right]^{\nu}, \end{aligned} \tag{S39}$$

where $n = N/\Omega$, $k_\pm = K_\pm/\Omega$ and the proportional factor is the normalization constant. In the public good scenario, $b > 0$, the F-conditional LNA-PDF is $p^*_{\mathrm{LNA},0}(N)$ while PDF conditioned on fixation of species S (but unconditioned on ξ) is proportional to $\pi^*(n)$ with $q = b$, i.e. it is given by

$$\begin{aligned} p^*_{\mathrm{LNA},\nu,b}(N) \quad \propto \quad & \int \frac{d\eta\; e^{-\eta^2/[2(n-\eta/\sqrt{\Omega})]}}{\left(n-\frac{\eta}{\sqrt{\Omega}}\right)^{3/2}\left(\psi^*_+ - \left(n-\frac{\eta}{\sqrt{\Omega}}\right)\right)} \left[\frac{\left\{\psi^*_+ - \left(n-\frac{\eta}{\sqrt{\Omega}}\right)\right\}\left\{\left(n-\frac{\eta}{\sqrt{\Omega}}\right) - \psi^*_-\right\}}{\left(n-\frac{\eta}{\sqrt{\Omega}}\right)^2}\right]^{\frac{\nu}{1+b}} \\ + \quad & \int \frac{d\eta\; e^{-\eta^2/[2(n-\eta/\sqrt{\Omega})]}}{\left(n-\frac{\eta}{\sqrt{\Omega}}\right)^{3/2}\left(\left(n-\frac{\eta}{\sqrt{\Omega}}\right) - \psi^*_-\right)} \left[\frac{\left\{\psi^*_+ - \left(n-\frac{\eta}{\sqrt{\Omega}}\right)\right\}\left\{\left(n-\frac{\eta}{\sqrt{\Omega}}\right) - \psi^*_-\right\}}{\left(n-\frac{\eta}{\sqrt{\Omega}}\right)^2}\right]^{\frac{\nu}{1+b}}, \end{aligned} \tag{S40}$$

where $\psi^*_+ = (1+b)k_+$ and $\psi^*_- = (1+b)k_-$.

The comparison between the LNA-PDFs and the $N-$QSD is shown in figures 7 and 8 of the main text, where a remarkable agreement is found when $b = 0$ and $b > 0$. However, as mentioned in the main text, some small deviations are observed in figure 8(a), at low switching rate, near the peak of small intensity when $b > 0$. The possible reasons for these small deviations are multiple: When $\nu \ll 1$, the population near the peaks of weak intensity is of size $N \approx (1+b)K_\pm$, and the assumption $\pi(\eta|\psi,\xi) \simeq \pi(\eta|\psi,-\xi)$ on which our LNA analysis is based may not be necessarily valid since the fluctuations in the state $\xi = -1$ (with $N \approx (1+b)K_-$ and $b = 2$) may be noticeably stronger than those in the state $\xi = +1$ (where $N \approx (1+b)K_+$). Furthermore, the peak in question is associated with the fixation of species S for $b = 2$ in a population of rather large size $\approx (1+b)K_+$, an event which occurs with a small probability that may be beyond the reach of the LNA. Moreover, the effective theory yielding the approximation $\phi \simeq \phi_q$ is based on the behavior at high switching rate and may be less accurate when $\nu \ll 1$ than in the regimes of intermediate and fast switching.

References

[1] Assaf M, Mobilia M, Roberts E. 2013 Cooperation Dilemma in Finite Populations under Fluctuating Environments. *Phys. Rev. Lett.* **111**, 238101. (doi: 10.1103/PhysRevLett.111.238101)

[2] Horsthemke W, Lefever R. 2006 *Noise-Induced Transitions*. Berlin, Germany: Springer

[3] Bena I. 2006 Dichotomous Markov noise: Exact results for out-of-equilibrium systems. A review. *Int. J. Mod. Phys. B* **20**, 2825-2889. (doi:10.1142/S0217979206034881)

[4] Davis M H A. 1984 Piecewise–deterministic Markov processes: a general class of nondiffusion stochastic models *J. R. Stat. Soc. B* **46**, 353-388. (Retrieved from http://www.jstor.org/stable/2345677)

[5] Kitahara K, Horsthemke W, Lefever R. 1979 Coloured-noise-induced transitions: exact results for external dichotomous Markovian noise. *Phys. Lett.* **70A**, 377-380. (doi: 10.1016/0375-9601(79)90336-0)

[6] Wolfram Research. 2010 Mathematica, Version 10.0 *Wolfram Research Inc*

[7] Wienand K, Frey E, Mobilia M. 2018 *Supplementary Material. fighshare https://doi.org/10.6084/m9.figshare.5683762*. (doi:10.6084/m9.figshare.5683762)

[8] Gillespie D T. 1976 A general method for numerically simulating the stochastic time evolution of coupled chemical reactions. *J. Comput. Phys.* **22**, 403. (doi: 10.1016/0021-9991(76)90041-3)

[9] A finite population unavoidably collapses into $(N, x) = (0, 0)$ where it is extinct [10]. This phenomenon is practically unobservable when $K_- \gg 1$ as it occurs after lingering in the system's quasi-stationary state (where N is distributed according to its N-QSD) and much after the fixation of one species.

[10] Spalding C, Doering C R, Flierl G R. 2017 Resonant activation of population extinctions *Phys. Rev. E* **96**, 042411. (doi: 10.1103/PhysRevE.96.042411)

[11] Hufton P G, Lin Y T, Galla T, McKane A J. 2016 Intrinsic noise in systems with switching environments. *Phys. Rev. E* **93**, 052119. (doi: 10.1103/PhysRevE.93.052119)

[12] Wienand K, Frey E, Mobilia M. 2017 Evolution of a Fluctuating Population in a Randomly Switching Environment. *Phys. Rev. Lett.* **119**, 158301. (doi:10.1103/PhysRevLett.119.158301)

[13] Wienand K, Frey E, Mobilia M. 2017 *http://link.aps.org/supplemental/10.1103/PhysRevLett.119.158301*. (doi: 10.1103/PhysRevLett.119.158301)

[14] Crow J F, Kimura M, 2009 *An Introduction to Population Genetics Theory*. New Jersey, USA: Blackburn Press

[15] Ewens E W, 2004 *Mathematical Population Genetics*. New York, USA: Springer.

[16] Antal I, Scheuring I. 2006 Fixation of Strategies for an Evolutionary Game in Finite Populations *Bull. Math. Biol.* **68**, 1923-1944. (doi: 10.1007/s11538-006-9061-4)

[17] Blythe R A, McKane A J. 2007 Stochastic models of evolution in genetics, ecology and linguistics *J. Stat. Mech.* **P07018** (doi:10.1088/17442-5468/2007/07/P07018)

[18] Cremer J, Reichenbach T, Frey E. 2009 The edge of neutral evolution in social dilemmas *New J. Phys.* **11**, 093029. (doi: 10.1088/1367-2630/11/9/093029)

[19] Gardiner C W. 2002 *Handbook of Stochastic Methods* New York, USA: Springer

[20] van Kampen N G. 2003 *Stochastic Processes in Physics and Chemistry* Amsterdam, The Netherlands: North-Holland Publishing

[21] Wienand K, Frey E, Mobilia M. 2017 *fighshare https://doi.org/10.6084/m9.figshare.5082712*. (doi:10.6084/m9.figshare.5082712.v5)

[22] Nowak M A, 2006 *Evolutionary Dynamics*. Cambridge, USA: Belknap Press

[23] Broom M, Rychtář J. 2013. *Game-Theoretical Models in Biology*. Boca Raton, USA: CRC Press